Mechatronics 22 (2012) 491–502

Contents lists available at SciVerse ScienceDirect

Mechatronics

journal homepage: www.elsevier.com/locate/mechatronics

Visual control with adaptive dynamical compensation for 3D target tracking by mobile manipulators

Víctor Andaluz [a], Ricardo Carelli [a,b], Lucio Salinas [a,b], Juan Marcos Toibero [a,b,*], Flavio Roberti [a,b]

[a] Instituto de Automática, Universidad Nacional de San Juan, Argentina
[b] Consejo Nacional de Investigaciones Científicas y Técnicas, Argentina

ARTICLE INFO

Article history:
Available online 24 October 2011

Keywords:
Visual control
Mobile manipulator
Stability analysis
3D target tracking

ABSTRACT

In this paper an image-based dynamic visual feedback control for mobile manipulators is presented to solve the target tracking problem in the 3D-workspace. The design of the whole controller is based on two cascaded subsystems: a minimum norm visual kinematic controller which complies with the 3D target tracking objective, and an adaptive controller that compensates the dynamics of the mobile manipulator. Both the kinematic controller and the adaptive controller are designed to prevent from command saturation. Robot commands are defined in terms of reference velocities. Stability and robustness are proved by using Lyapunov's method. Finally, experimental results are presented to confirm the effectiveness of the proposed visual feedback controller.

1. Introduction

In recent years, robotics research has experienced a significant change. The research interests are moving from the development of robots for structured industrial environments to the development of autonomous mobile robots operating in unstructured and natural environments. These autonomous mobile robots are applicable in a number of challenging tasks such as cleaning of hazardous material, surveillance, rescue and reconnaissance in unstructured environments where humans are kept away from. Since it is foreseen that this new class of mobile robots will have extensive applications in activities where human capabilities are needed, they have attracted the attention of the researchers [1]. Mobile manipulator robot is nowadays a widespread term that refers to robots composed of a robotic arm mounted on a mobile platform. This kind of system, which is usually characterized by a high degree of redundancy, combines the manipulability of a fixed-base manipulator with the mobility of a wheeled platform. Such systems allow the most usual missions of robotic systems which required both *locomotion* and *manipulation* abilities. Such systems offer multiple applications in different industrial and productive areas as mining and construction or for people assistance [2,3].

Robots and intelligent machines need large amounts of information to autonomously deal with objects in dynamical environments. Visual information has proven to be a highly effective means for recognizing unknown surroundings. Vision is a useful robotic sensor since it mimics the human sense of vision and allows for noncontact measurement of the environment. Visual feedback control of robotic systems involves the fusion of robot kinematics, dynamics, and computer vision to control the motion of the robot in an efficient manner. Visual feedback control is classified into two groups, position based control and image-based control [4]. In position-based control, the references are given in the three-dimensional Cartesian space. The control objective is to bring a relative pose, which is the pose from a camera to a target or from a hand to a target, to a desired pose by using image information. In image-based control, the references are given in the image plane.

A new tendency is to integrate visual servoing into mobile robots for grasping or manipulation, resulting in a vision-based autonomous mobile manipulation system [5–11]. Ref. [5] has developed an image-based visual servo controller for nonholonomic mobile manipulators. In this paper, two well-known methods of redundancy resolution for fixed-base manipulators are extended for kinematics modelling of a specific nonholonomic mobile manipulator. The proposed approach is illustrated only through computer simulation. In [6], authors present a framework of hand–eye relation for visual servoing with a more global view. In this case two mobile manipulators are used, for the main robot the camera architecture is eye-to-hand configuration, and eye-in-hand configuration for the second robot. Ref. [7] presents a robust vision-based mobile manipulation system for wheeled mobile robots (WMRs). This paper addresses the retention of visual features in the field of view of the camera. A hybrid controller for mobile manipulation is developed to integrate the IBVS controller and the Q-learning controller through a rule-based supervisor.

* Corresponding author at: Instituto de Automática, Universidad Nacional de San Juan, Argentina. Tel.: +54 264 4213303; fax: +54 264 4213672.
E-mail addresses: vandaluz@inaut.unsj.edu.ar (V. Andaluz), mtoibero@inaut.unsj.edu.ar (J.M. Toibero).

0957-4158/$ - see front matter © 2011 Elsevier Ltd. All rights reserved.
doi:10.1016/j.mechatronics.2011.09.013

In order to reduce performance degradation, on-line parameter adaptation becomes quite important in applications where the mobile manipulator dynamic parameters may vary, such as load transportation. It is also useful when there is uncertainty in the knowledge of the dynamic parameters.

In this paper, it is considered a robotic arm mounted on a nonholonomic mobile platform. The mobile manipulator dynamic model [12] has, differently to previous works, reference velocities as input signals as it is common in commercial robots. It is then presented a visual servo controller with adaptive compensation, designed for 3D target tracking by mobile manipulators with eye-in-hand configuration. This controller sets the mobile manipulator's internal configuration and provides the robot the capability to avoid obstacles in its path. The design of the controller is based on two parts, each one being a controller itself. The first one is a minimum norm visual servo controller which avoids saturations of the velocity commands. It is based on both the mobile manipulator's kinematic model and the vision system model. The second one is an adaptive dynamic compensation controller, which receives as inputs the velocity references calculated by the kinematic controller. The adaptive dynamic compensation controller is capable of updating the estimated parameters, which are directly related to physical parameters of the mobile manipulator. Additionally, it is proved the stability and robustness properties to parametric uncertainties in the dynamic model by using the Lyapunov's method [13]. To validate the proposed control algorithms, experimental results are included and discussed.

The main contributions of this paper are: (a) It presents an image-based visual control for 3D target tracking of mobile manipulators. The controller receives both the estimation of the object's velocity to be followed and the error image feature to calculate the control commands as velocity references for the platform and for the arm, thus achieving a coordinated movement of the whole system. Also, the controller is designed including saturation functions to limit the control actions within its physical bounds. (b) Two secondary objectives are included in the kinematics controller design by handling the redundancy of the system: the avoidance of obstacles by the mobile platform and the maximum manipulability during task execution. (c) The design of an adaptive controller to reduce the dynamic parameter uncertainty effects.

This paper is organized as follows. Section 2 presents the kinematic and dynamic models which have as inputs the velocities of the mobile manipulator. Also included in this Section is the projection model of the vision camera. Next, in Section 3, the problem formulation, the vision-based control strategy for the mobile manipulation system and the design of the kinematic and adaptive dynamic compensation controllers are presented. In Section 4, it is developed the control system stability and robustness analysis. The Experimental results are presented and discussed in Section 5. Finally, conclusions are given in Section 6.

2. Mobile manipulator models

The mobile manipulator configuration is defined by a vector $\mathbf{q}$ of n independent coordinates, called *generalized coordinates of the mobile manipulator*, where $\mathbf{q} = [\,q_1 \quad q_2 \quad \dots \quad q_n\,]^T = [\,\mathbf{q}_p^T \quad \mathbf{q}_a^T\,]^T$. We notice that $n = n_p + n_a$, where n_p and n_a are respectively the dimensions of the generalized spaces associated to the mobile platform and to the robotic arm. The configuration $\mathbf{q}$ is an element of the *configuration space* of the mobile manipulator, denoted by N. The location of the end-effector of the mobile manipulator is given by the m -dimensional vector $\mathbf{h} = [\,h_1 \quad h_2 \quad \dots \quad h_m\,]^T$. Its m coordinates are *operational coordinates of the mobile manipulator*. They define the position and the orientation of the end-effector in R. The set of all the locations constitutes the *operational space of the mobile manipulator*, denoted by M.

The location of the end-effector of the mobile manipulator can be defined in different ways according to the task, *i.e.*, it can be considered only the position of the end-effector or both its position and orientation.

2.1. Kinematic model of the mobile manipulator

The *kinematic model of a mobile manipulator* represents the location of its end-effector $\mathbf{h}$ as a function of the robotic arm configuration and of the platform location (or its operational coordinates as functions of the robotic arm generalized coordinates and of the mobile platform operational coordinates) [25].

$$\{ : \mathcal{N}_{\dashv} \times \mathcal{M}_{\surd} \rightarrow \mathcal{M}$$
$$(\mathbf{q}_p, \mathbf{q}_a) \mapsto \mathbf{h} = \{(\mathbf{q}_p, \mathbf{q}_a)$$

where, N_a is the *configuration space* of the robotic arm, M_p is the *operational space of the platform.*

The *instantaneous kinematic model of a mobile manipulator*gives the derivative of its end-effector location as a function of the derivatives of both the robotic arm configuration and the location of the mobile platform,

$$\dot{\mathbf{h}} = \frac{\partial f}{\partial \mathbf{q}}(\mathbf{q}_p, \mathbf{q}_a)\mathbf{v}$$

where, $\dot{\mathbf{h}} = \left[\,\dot{h}_1 \quad \dot{h}_2 \quad \dots \quad \dot{h}_m\,\right]^T$ is the vector of the end-effector velocity, $\mathbf{v} = [\,v_1 \quad v_2 \quad \dots \quad v_{\delta_n}\,]^T = [\,v_p^T \quad v_a^T\,]^T$ is the control vector of mobility of the mobile manipulator. Its dimension is $\delta_n = \delta_{np} + \delta_{na}$, where δ_{np} and δ_{na} are respectively the dimensions of the control vector of mobility associated to the mobile platform and to the robotic arm. Now, after replacing $\mathbf{J_g}(\mathbf{q}) = \frac{\partial f}{\partial \mathbf{q}}(\mathbf{q}_p, \mathbf{q}_a)$ in the above equation, it is obtained

$$\dot{\mathbf{h}}(t) = \mathbf{J_g}(\mathbf{q})\mathbf{v}(t) \tag{1}$$

where, $\mathbf{J_g}(\mathbf{q})$ is the Jacobian matrix that defines a linear mapping between the vector of the mobile manipulator velocities $\mathbf{v}(\boldsymbol{t})$ and the vector of the end-effector velocity $\dot{\mathbf{h}}(\boldsymbol{t})$. The Jacobian matrix is, in general, a function of the configuration $\mathbf{q}$; those configurations at which $\mathbf{J_g(q)}$ is rank-deficient are termed *singular kinematic configurations*. It is fundamental to notice that, in general, the dimension of operational space m is less than the degree of mobility of the mobile manipulator. In this case the problem, including the mobile manipulator and the task, is called to be redundant.

2.2. Dynamic model of the mobile manipulator

The mathematic model that represents the dynamics of a mobile manipulator can be obtained from Lagrange's dynamic equations, which are based on the difference between the kinetic and potential energy of each of the joints of the robot (energy balance) [14]. The dynamic equation of the mobile manipulator can be represented according to [15] as follows,

$$\mathbf{M}(\mathbf{q})\dot{\mathbf{v}} + \mathbf{C}(\mathbf{q}, \mathbf{v})\mathbf{v} + \mathbf{G}(\mathbf{q}) = \mathbf{B}(\mathbf{q})\boldsymbol{\tau}$$

where, $\mathbf{M}(\mathbf{q}) \in \Re^{\delta_n \times \delta_n}$ is a symmetrical positive definite matrix that represents the system's inertia, $\mathbf{C}(\mathbf{q}, \mathbf{v})\mathbf{v} \in \Re^{\delta_n}$ represents the components of the centripetal and Coriolis forces, $\mathbf{G}(\mathbf{q}) \in \Re^{\delta_n}$ represents the gravitational forces, $\mathbf{B}(\mathbf{q})$ is the input transformation matrix and $\boldsymbol{\tau} \in \Re^{\delta_n}$ is the torque input vector. For more details on the model see [15].

Most of the commercially available robots have low level PID controllers in order to follow the reference velocity inputs, thus not allowing controlling the voltages of the motors directly. There-

fore, it becomes useful to express the dynamic model of the mobile manipulator in a more appropriate way, taking the rotational and longitudinal reference velocities as the control signals. To do so, the velocity servo controller dynamics are included in the model. The dynamic model of the mobile manipulator, having as control signals the reference velocities of the system, can be represented as follows,

$$\overline{\mathbf{M}}(\mathbf{q})\dot{\mathbf{v}} + \overline{\mathbf{C}}(\mathbf{q},\mathbf{v})\mathbf{v} + \overline{\mathbf{G}}(\mathbf{q}) = \mathbf{v}_{\mathbf{ref}} \tag{2}$$

where $\overline{\mathbf{M}}(\mathbf{q}) = \mathbf{H}^{-1}(\mathbf{M}+\mathbf{D}), \overline{\mathbf{C}}(\mathbf{q},\mathbf{v}) = \mathbf{H}^{-1}(\mathbf{C}+\mathbf{P}), \overline{\mathbf{G}}(\mathbf{q}) = \mathbf{H}^{-1}\mathbf{G}(\mathbf{q})$. Thus, $\overline{\mathbf{M}}(\mathbf{q}) \in \Re^{\delta_n \times \delta_n}$ is a positive definite matrix, $\overline{\mathbf{C}}(\mathbf{q},\mathbf{v})\mathbf{v} \in \Re^{\delta_n}, \overline{\mathbf{G}}(\mathbf{q}) \in \Re^{\delta_n}$ and $\mathbf{v}_{\mathbf{ref}} \in \Re^{\delta_n}$ is the vector of velocity control signals, $\mathbf{H} \in \Re^{\delta_n \times \delta_n}, \mathbf{D} \in \Re^{\delta_n \times \delta_n}$ and $\mathbf{P} \in \Re^{\delta_n \times \delta_n}$ are symmetrical diagonal matrices, positive definite, that contain the physical parameters of the mobile manipulator, motors, velocity controllers of both the mobile platform and the manipulator robot.

Property 1. *Matrix* $\overline{\mathbf{M}}$ *is positive definite, additionally it is known that*

$$\|\overline{\mathbf{M}}(\mathbf{q})\| < k_M$$

Property 2. *Furthermore, the following inequalities are also satisfied*

$$\|\overline{\mathbf{C}}(\mathbf{q},\mathbf{v})\| < k_c\|\mathbf{v}\|$$

Property 3. *Vector* $\overline{\mathbf{G}}(\mathbf{q})$ *is bounded*

$$\|\overline{\mathbf{G}}(\mathbf{q})\| < k_G$$

where, k_c, k_M *and* k_G *denote some positive constants.*

Property 4. *The dynamic model of the mobile manipulator can be represented by*

$$\overline{\mathbf{M}}(\mathbf{q})\dot{\mathbf{v}} + \overline{\mathbf{C}}(\mathbf{q},\mathbf{v})\mathbf{v} + \overline{\mathbf{G}}(\mathbf{q}) = \mathbf{L}(\mathbf{q},\mathbf{v})\boldsymbol{\chi}$$

where, $\mathbf{L}(\mathbf{q},\mathbf{v})\chi \in \Re^{\delta_n \times l}$ *and* $\chi = [\chi_1\ \chi_2\ \ldots\ \chi_l]^T$ *is the vector of l unknown parameters of the mobile manipulator, i.e., mass of the mobile robot, mass of the robotic arm, physical parameters of the mobile manipulator, motors, velocity, etc. For more details on the model see [12].*

For the sake of simplicity, from now on it will be written $\overline{\mathbf{M}} = \overline{\mathbf{M}}(\mathbf{q})$, $\overline{\mathbf{C}} = \overline{\mathbf{C}}(\mathbf{q},\mathbf{v})$ and $\overline{\mathbf{G}} = \overline{\mathbf{G}}(\mathbf{q})$.

The full mathematical model of the mobile manipulator system is represented by: (1) the *kinematic model* and (2) the *dynamic model,* taking the reference velocities of the system as control signals.

2.3. Camera projection model

To control the robot using information provided by a computer vision system, it is necessary to understand the geometric aspects of the imaging process. Each camera contains a lens that forms a 2D projection of the scene on the image plane where the sensor is located. This projection causes the loss of direct depth perception so that each point on the image plane corresponds to a ray in 3D space. Therefore, some additional information is needed to determine the 3D coordinates corresponding to an image plane point. This information may come from multiple cameras, multiple views with a single camera, or knowledge of the geometric relationship between several feature points on the target. The camera model used in this paper is the perspective projection model or *pinhole model.* It implies a simplified model for an ideal vision camera without distortion and optical aberrations.

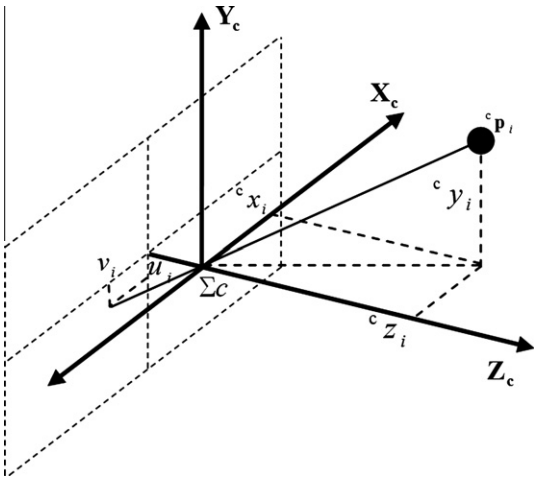

Fig. 1. Pinhole camera model.

The pinhole camera model with a perspective projection is shown in Fig. 1. Let f_c be a focal length, ${}^{w}\mathbf{p}_i \in \Re^3$ and ${}^{c}\mathbf{p}_i = [{}^{c}x_i\ \ {}^{c}y_i\ \ {}^{c}z_i]^T \in \Re^3$ be the 3D position vectors of the target object's *i*th feature point relative to Σo and Σc, respectively. Σo represents the world framework and Σc is the camera (end-effector) framework, as Fig. 2 shows. Using a coordinate transformation, the relation between them is,

$${}^{c}\mathbf{p}_i = {}^{c}\mathbf{R}_w({}^{w}\mathbf{p}_i - {}^{w}\mathbf{p}_{Corg}) \tag{3}$$

The perspective projection of the *i* – th feature point onto the image plane gives us the image plane coordinate $\xi_i = [u_i\ \ v_i]^T \in \Re^2$ as

$$\xi_i({}^{c}x_i, {}^{c}y_i, {}^{c}z_i) = -\frac{f_c}{{}^{c}z_i}\begin{bmatrix} {}^{c}x_i \\ {}^{c}y_i \end{bmatrix} \tag{4}$$

Differentiating (3) and (4), it can be expressed $\dot{\xi}_i$ in terms of the mobile manipulator velocity as

$$\dot{\xi}_i = \mathbf{J}_{\mathbf{I}_i}(\xi_i, {}^{c}z_i)\begin{bmatrix} {}^{c}\mathbf{R}_w & 0 \\ 0 & {}^{c}\mathbf{R}_w \end{bmatrix}\mathbf{J}_{\mathbf{g}}(\mathbf{q})\mathbf{v} - \mathbf{J}_{\mathbf{o}_i}(\mathbf{q}, {}^{c}\mathbf{p}_i)^{w}\dot{\mathbf{p}}_i \tag{5}$$

where $\mathbf{J}_{\mathbf{g}}(\mathbf{q})$ is the *geometric Jacobian* of the mobile manipulator defined in (1), $\mathbf{J}_{\mathbf{I}_i}(\xi_i, {}^{c}z_i)$ is the *image Jacobian* defined by

$$\mathbf{J}_{\mathbf{I}_i}(\xi_i, {}^{c}z_i) = \begin{bmatrix} \frac{f_c}{{}^{c}z_i} & 0 & \frac{u_i}{{}^{c}z_i} & \frac{u_i v_i}{f_c} & \frac{f_c^2+u_i^2}{f_c} & v_i \\ 0 & \frac{f_c}{{}^{c}z_i} & \frac{v_i}{{}^{c}z_i} & \frac{f_c^2+v_i^2}{f_c} & \frac{u_i v_i}{f_c} & -u_i \end{bmatrix}$$

Moreover, $\mathbf{J}_{\mathbf{o}_i}(\mathbf{q}, {}^{c}\mathbf{p}_i)^{w}\dot{\mathbf{p}}_i$ represents the movement of the *i*th feature point into the image plane, where ${}^{w}\dot{\mathbf{p}}_i$ is the velocity of the *i* – th feature point relative to Σo and $\mathbf{J}_{\mathbf{o}_i}(\mathbf{q}, {}^{c}\mathbf{p}_i)$ is defined as

$$\mathbf{J}_{\mathbf{o}i}(\mathbf{q}, {}^{c}\mathbf{p}_i) = \frac{f_c}{{}^{c}z_i}\begin{bmatrix} 1 & 0 & -\frac{{}^{c}x_i}{{}^{c}z_i} \\ 0 & 1 & -\frac{{}^{c}y_i}{{}^{c}z_i} \end{bmatrix}{}^{c}\mathbf{R}_w$$

In applications where objects are located in a 3D space, three or more image features are required for the visual servo control to be solvable [16,17]. To extend this model to *r* image points it is necessary to stack the vectors of the image plane coordinate, *i.e.*,

$$\xi = [\xi_1^T\ \ \xi_2^T\ \ \ldots\ \ \xi_r^T]^T \in \Re^{2r} \tag{6}$$

and ${}^{c}\mathbf{p} = [{}^{c}\mathbf{p}_1\ \ {}^{c}\mathbf{p}_2\ \ \ldots\ \ {}^{c}\mathbf{p}_r]^T \in \Re^{3r}$. It is assumed that multiple point features on a known object are given. From Eq. (5), for multiple point features it can be written

$$\dot{\xi} = \mathbf{J}(\mathbf{q}, \xi, {}^{c}z)\mathbf{v} - \mathbf{J}_{\mathbf{o}}(\mathbf{q}, {}^{c}\mathbf{p})^{w}\dot{\mathbf{p}} \tag{7}$$

where

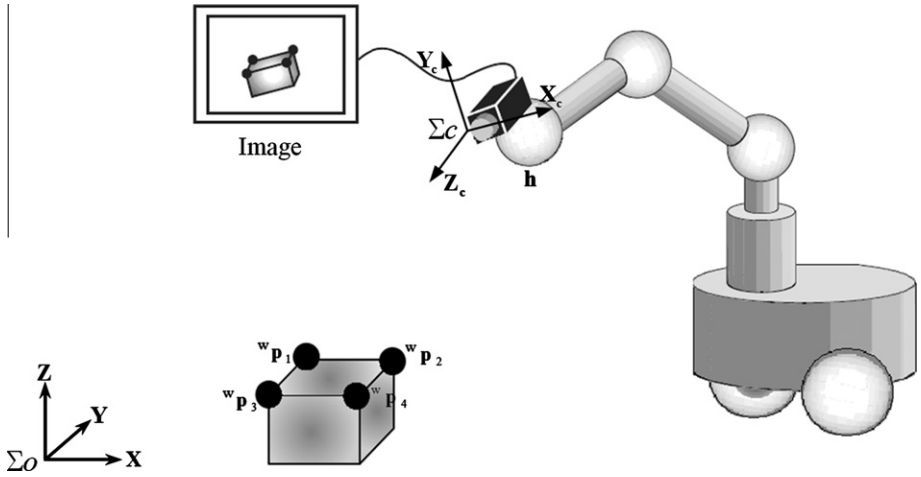

Fig. 2. Framework for a dynamic visual feedback system for redundant mobile manipulator.

$$\mathbf{J}(\mathbf{q},\xi,{}^{c}z)=\mathbf{J}_{\mathbf{I}}(\xi,{}^{c}z)\begin{bmatrix}{}^{c}\mathbf{R}_{w} & 0\\ 0 & {}^{c}\mathbf{R}_{w}\end{bmatrix}\mathbf{J}_{g}(\mathbf{q})$$

$$\mathbf{J}_{\mathbf{I}}(\xi,{}^{c}z)=\begin{bmatrix}\mathbf{J}_{1}\left(\begin{bmatrix}u_1 & v_1\end{bmatrix}^{T},{}^{c}z_1\right)\\ \vdots\\ \mathbf{J}_{r}\left(\begin{bmatrix}u_r & v_r\end{bmatrix}^{T},{}^{c}z_r\right)\end{bmatrix}$$

$$\mathbf{J}_{\mathbf{o}}(\mathbf{q},{}^{c}\mathbf{p})=\begin{bmatrix}\frac{f_c}{{}^{c}z_1}\begin{bmatrix}1 & 0 & -\frac{{}^{c}x_1}{{}^{c}z_1}\\ 0 & 1 & -\frac{{}^{c}y_1}{{}^{c}z_1}\end{bmatrix} & \cdots & \frac{f_c}{{}^{c}z_m}\begin{bmatrix}1 & 0 & -\frac{{}^{c}x_r}{{}^{c}z_r}\\ 0 & 1 & -\frac{{}^{c}y_r}{{}^{c}z_r}\end{bmatrix}\end{bmatrix}^{T}{}^{c}\mathbf{R}_{w}$$

For the sake of simplicity, from now on it will be used the following notation $\mathbf{J}=\mathbf{J}(\mathbf{q},\xi,{}^{c}z)$ and $\mathbf{J_o}=\mathbf{J_o}(\mathbf{q},{}^{c}\mathbf{p})$.

3. Control problem formulation and controllers design

The mobile manipulator robot task is specified in the image plane in terms of the image feature values corresponding to the relative robot and object positions. Let us denote with $\xi_d \in \Re^{2r}$ the *desired image feature*vector which is assumed to be constant. For some tasks, the desired feature vector ξ_d can be obtained directly in the image feature space. Another way to get ξ_d is by using a "teach-by-showing" strategy [18]. In this approach, an image is captured at the desired reference position and the corresponding extracted features represent the desired feature vector ξ_d. The control problem is to design a controller which computes the applied velocities $\mathbf{v_{ref}}$ to move the mobile manipulator in such a way that the actual image features reach the prescribed desired ones. The proposed control scheme to solve the visual control problem is shown in Fig. 3. The design of the controller is based on two cascaded subsystems.

(1) Minimum norm kinematic controller with saturation of velocity commands, where the image feature error defined as $\tilde{\xi}=\xi_d-\xi$ may be calculated at every measurement time and used to drive the mobile manipulator in a direction which decreases the error. Therefore, the control aim is to ensure that

$$\lim_{t\to\infty}\tilde{\xi}(t)=\mathbf{0}\in\Re^{2r}$$

(2) Adaptive dynamic compensation controller, which main objective is to compensate the dynamics of the mobile manipulator thus reducing the velocity tracking error. This controller receives as inputs the desired velocities $\mathbf{v_c}$ calculated by the kinematic controller, and generates velocity references $\mathbf{v_{ref}}$ for the mobile manipulator robot. The velocity control error is defined as $\tilde{\mathbf{v}}=\mathbf{v_c}-\mathbf{v}$. Hence, the control aim is to ensure that

$$\lim_{t\to\infty}\tilde{\mathbf{v}}(t)=\mathbf{0}\in\Re^{\delta_n}$$

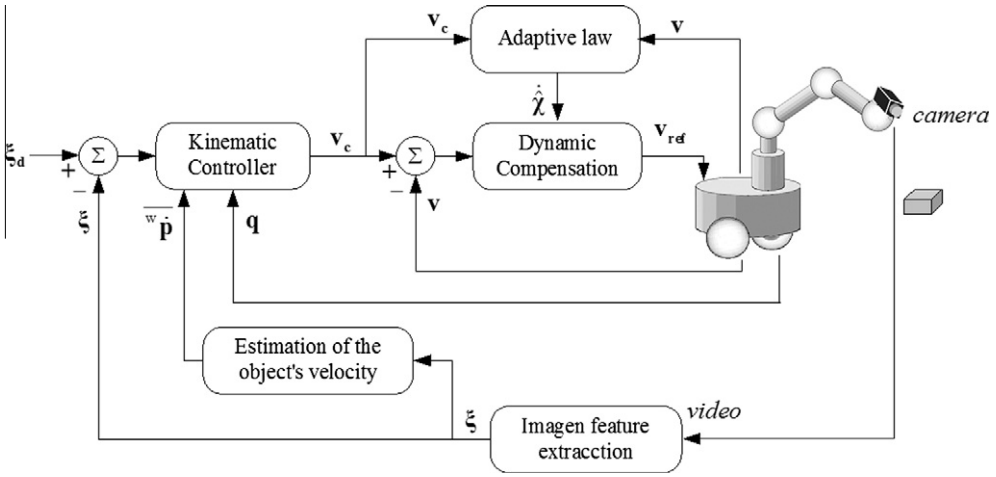

Fig. 3. Dynamic visual control for 3D target tracking of mobile manipulators.

3.1. Minimal norm kinematic controller

The design of the kinematic controller is based on the kinematic model of the mobile manipulator and camera projection model. From (7), $\mathbf{v}$ can be expressed in terms of $\dot{\xi}$ and ${}^{w}\dot{\mathbf{p}}$ by using the right pseudo-inverse of the matrix $\mathbf{J}$

$$\mathbf{v} = \mathbf{J}^{\#}(\dot{\xi} + \mathbf{J_o}{}^{w}\dot{\mathbf{p}})$$

where, $\mathbf{J}^{\#} = \mathbf{W}^{-1}\mathbf{J}^{T}(\mathbf{J}\mathbf{W}^{-1}\mathbf{J}^{T})^{-1}$, being $\mathbf{W}$ a positive definite matrix that weighs the control actions of the system,

$$\mathbf{v} = \mathbf{W}^{-1}\mathbf{J}^{T}(\mathbf{J}\mathbf{W}^{-1}\mathbf{J}^{T})^{-1}(\dot{\xi} + \mathbf{J_o}{}^{w}\dot{\mathbf{p}}) \tag{8}$$

The controller is based on a minimal norm solution, which means that, at any time, the mobile manipulator will attain its navigation target with the smallest number of possible movements. Also the redundancy of the mobile manipulators is effectively used for achieving secondary control objectives, such as: avoiding obstacles in the workspace and to control the mobile manipulator's configuration. The following control law is proposed for the visual control of the mobile manipulator system,

$$\mathbf{v_c} = \mathbf{J}^{\#}(\mathbf{J_o}{}^{w}\dot{\mathbf{p}} + \mathbf{L_K}\tanh\left(\mathbf{L_K^{-1}}\mathbf{K}\tilde{\xi}\right)) + (\mathbf{I} - \mathbf{J}^{\#}\mathbf{J})\mathbf{L_D}\tanh\left(\mathbf{L_D^{-1}}\mathbf{D}\mathbf{v}_0\right) \tag{9}$$

In (9), $\mathbf{J_o}{}^{w}\dot{\mathbf{p}}$ represents the velocity of the object to be followed into the image plane, $\tilde{\xi}$ is the vector of control errors defined as $\tilde{\xi} = \xi_d - \xi, \mathbf{K} \in \Re^{2r}, \mathbf{D} \in \Re^{\delta}, \mathbf{L_K} \in \Re^{2r}$ and $\mathbf{L_D} \in \Re^{\delta}$ are definite positive diagonal matrices that weigh the error vector $\tilde{\xi}$ and the vector $\mathbf{v}_0$, where $\mathbf{v}_0 \in \Re^{\delta}$ is an arbitrary vector which contains the velocities associated to the mobile manipulator. The first term of the right hand side in (9) describes the primary task of the end effector, i.e., to achieve the desired image features values in order to track the moving object. The second term defines self motion of the mobile manipulator in which the matrix $(\mathbf{I} - \mathbf{J}^{\#}\mathbf{J})$ projects vector $\mathbf{v}_0$ onto the null space of the manipulator Jacobian $N(\mathbf{J})$. This way, the secondary control objectives do not affect the primary task of the end-effector. Therefore, any value given to $\mathbf{v}_0$ will only change the internal structure of the manipulator without changing the end-effector location. Thus, the redundancy of the mobile manipulators can be effectively used for the achievement of additional performances such as: avoiding obstacles in the workspace, avoiding singular configurations, or to optimize various performance criteria. In this work two different secondary objectives are considered: the obstacles avoidance by the mobile platform and the singular configuration prevention through the system's manipulability control. These secondary objectives are described below.

3.1.1. Manipulability

We can observe that one of the main requirements for an accurate task execution by the robot is a good manipulability, defined as the robot configuration that maximizes its ability to manipulate a target object. Therefore, one of the secondary objectives of the control is to maintain maximum manipulability of the mobile manipulator during task execution. Manipulability is a concept introduced by Yoshikawa [19] to measure the ability of a fixed manipulator to move in certain directions. Bayle [20] presents a similar analysis for the manipulability of mobile manipulators and extends the concept of manipulability ellipsoid as the set of all end-effector velocities reachable by robot velocities $\mathbf{v}$ satisfying $\|\mathbf{v}\| \leqslant 1$ in the Euclidean space. A global representative measure of manipulation ability can be obtained by considering the volume of this ellipsoid which is proportional to the quantity w called the *manipulability measure*,

$$w = \sqrt{\det(\mathbf{J}(\mathbf{q})\mathbf{J}^{T}(\mathbf{q}))} \tag{10}$$

Therefore, the mobile manipulator will have maximum manipulability if its internal configuration is such that maximizes the manipulability measure w.

3.1.2. Obstacle avoidance

The main idea is to avoid obstacles which maximum height does not interfere with the robotic arm. Therefore the arm can follow the desired path while the mobile platform avoids the obstacle by resourcing to the null space configuration. Fig. 4 shows the obstacle avoidance strategy. The angular velocity and the longitudinal velocity of the mobile platform will be affected by a fictitious repulsion force. This force depends on both, the incidence angle on the obstacle α and the distance d to the obstacle. This way, the following control velocities are proposed:

$$u_{obs} = Z^{-1}(k_{uobs}(d_o - d)[\pi/2 - |\alpha|]) \tag{11}$$

$$\omega_{obs} = Z^{-1}(k_{\omega obs}(d_o - d)\mathrm{sign}(\alpha)[\pi/2 - |\alpha|]) \tag{12}$$

where, d_o is the radius which determines the distance at which the obstacle starts to be avoided, $k_{u\ obs}$ and $k_{\omega\ \mathrm{obs}}$ are positive adjustment gains, the sign function allows defining to which side the obstacle is to be avoided being sign $(0) = 1$. Z represents the mechanical impedance characterizing the robot-environment interaction, which is calculated as $Z = Is^2 + Bs + K$ with I, B and K being positive constants representing, respectively, the effect of virtual inertia, damping and elasticity. The closer the platform is to the obstacle, the bigger the values of ω_{obs} and u_{obs}.

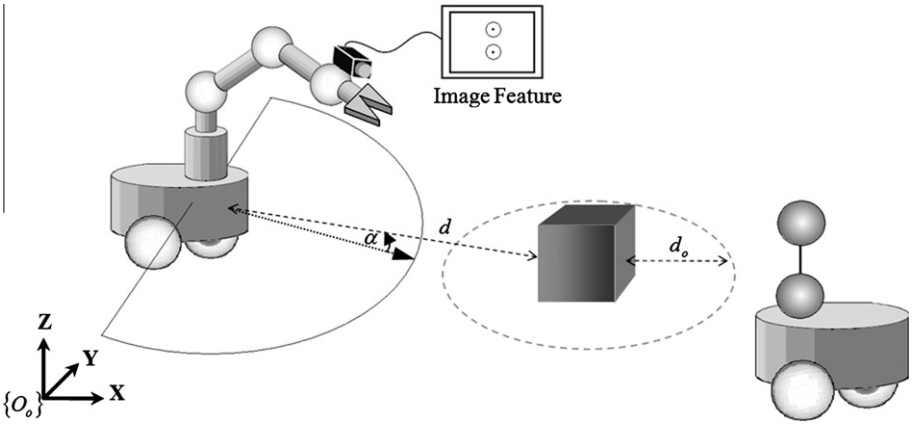

Fig. 4. Obstacle avoidance scheme.

Taking into account the maximum manipulability (10) and the obstacle avoidance (11) and (12), the vector $\mathbf{v}_0$ is now defined as,

$$\mathbf{v}_0 = [-u_{obs} \quad \omega_{obs} \quad k_{v1}(\theta_{1d} - \theta_1) \quad k_{v2}(\theta_{2d} - \theta_2) \quad \dots \quad k_{vna}(\theta_{nad} - \theta_{na})]^T$$

where $k_{vi}(\theta_{id} - \theta_i)$ – being $i = 1, 2, \dots, n_a$ and $k_{vi} > 0$ – are joint velocities proportional to the configuration errors of the mobile robotic arm, in such a way that the manipulator joints will be pulled to the desired θ_{id} values that maximize manipulability. Note that $-u_{obs}$ represents a reduction value for the linear velocity in order to obtain a cautious behaviour. For this reason, u_{obs} must be subtracted from the linear velocity component obtained in the first term of (9).

In order to include an analytical saturation of velocities in the mobile manipulator system, it is proposed the use of the tanh (.) function, which limits the error in $\tilde{\xi}$ and the magnitude of vector $\mathbf{v}_0$. The expressions $\tanh\left(\mathbf{L}_\mathbf{K}^{-1}\mathbf{K}\tilde{\mathbf{h}}\right)$ and $\tanh\left(\mathbf{L}_\mathbf{D}^{-1}\mathbf{D}\mathbf{v}_\mathbf{0}\right)$ denote a component by component operation.

3.1.3. Stability analysis of the kinematic controller

The behaviour of the control error $\tilde{\xi}$ is now analyzed assuming - by now- perfect velocity tracking $\mathbf{v} \equiv \mathbf{v_c}, \mathbf{v_c} = [u_c \quad \omega_c \quad \dot{\theta}_{1c} \quad \dot{\theta}_{2c} \dots \dot{\theta}_{nac}]^T$. Note that the desired image feature vector is constant, then it can be concluded that $\dot{\tilde{\xi}} = -\dot{\xi}$. Now, by substituting (9) in (7) the following closed loop equation is obtained

$$\dot{\tilde{\xi}} + \mathbf{L}_\mathbf{K} \tanh\left(\mathbf{L}_\mathbf{K}^{-1}\mathbf{K}\tilde{\xi}\right) = \mathbf{0} \tag{13}$$

For the stability analysis the following Lyapunov candidate function is considered

$$V(\tilde{\xi}) = \frac{1}{2}\tilde{\xi}^\mathbf{T}\tilde{\xi} \tag{14}$$

Its time derivative on the trajectories of the system is,

$$\dot{V}(\tilde{\xi}) = -\tilde{\xi}^\mathbf{T}\mathbf{L}_\mathbf{K} \tanh\left(\mathbf{L}_\mathbf{K}^{-1}\mathbf{K}\tilde{\xi}\right) < 0 \tag{15}$$

which implies that $\tilde{\xi}(t) \to \mathbf{0}$ asymptotically.

3.2. Adaptive dynamic compensation

The proposed kinematic controller presented in Section 3.A assumes perfect velocity tracking; nevertheless this is not true in real contexts, mainly when high-speed movements or heavy load transportation are required. Therefore, it becomes essential to consider the mobile manipulator dynamics, in addition to its kinematics. Furthermore, it is very important to consider that the dynamic parameters of the mobile manipulator may be uncertain due to changes in dynamics for different tasks. Hence, the velocity error due to the dynamic effects of the robot and the uncertainties of the real dynamic parameters of the mobile manipulator motivates to design an *adaptive dynamic compensation controller* with a robust parameter updating law, as shows Fig. 3.

The adaptive dynamic compensation controller receives as inputs the desired velocities $\mathbf{v_c}$ calculated by the kinematic controller, and generates velocity references $\mathbf{v_{ref}}$ for the mobile manipulator robot (see Fig. 3). Hence, disregarding the assumption of perfect velocity tracking, the velocity error is defined as,

$$\tilde{\mathbf{v}} = \mathbf{v_c} - \mathbf{v}$$

The proposed control law is,

$$\mathbf{v_{ref}} = \widehat{\overline{\mathbf{M}}}(\mathbf{q})\sigma + \widehat{\overline{\mathbf{C}}}(\mathbf{q}, \mathbf{v})\mathbf{v_c} + \widehat{\overline{\mathbf{G}}}(\mathbf{q}) \tag{16}$$

where, $\mathbf{v_{ref}} = [u_{ref} \quad \omega_{ref} \quad \dot{\theta}_{1ref} \quad \dot{\theta}_{2ref} \quad \dots \quad \dot{\theta}_{naref}]^T$; $\widehat{\overline{\mathbf{M}}}(\mathbf{q})$, $\widehat{\overline{\mathbf{C}}}(\mathbf{q}, \mathbf{v})$, $\widehat{\overline{\mathbf{G}}}(\mathbf{q})$ are de estimated model matrices; and

$$\sigma = \dot{\mathbf{v}}_\mathbf{c} + \mathbf{L}_\mathbf{v} \tanh(\mathbf{L}_\mathbf{v}^{-1}\mathbf{K}_\mathbf{v}\tilde{\mathbf{v}}) \tag{17}$$

with $\mathbf{K_v}$ and $\mathbf{L_v}$ symmetrical positive definite matrices.

Eq. (16) considering the Property 4 can also be written as

$$\mathbf{v_{ref}} = \mathbf{\Phi}(\mathbf{q}, \mathbf{v}, \boldsymbol{\sigma})\boldsymbol{\chi} \tag{18}$$

where, $\mathbf{\Phi}(\mathbf{q}, \mathbf{v}, \boldsymbol{\sigma})\boldsymbol{\chi} \in \Re^{\delta_n \times l}$ and $\boldsymbol{\chi} = [\chi_1 \ \chi_2 \ \dots \ \chi_l]$ is the vector of l unknown parameters of the mobile manipulator.

When such parametric errors are considered, control law (18) can be re-written as,

$$\mathbf{v_{ref}} = \mathbf{\Phi}\hat{\boldsymbol{\chi}} = \mathbf{\Phi}\boldsymbol{\chi} + \mathbf{\Phi}\tilde{\boldsymbol{\chi}} = \overline{\mathbf{M}}\boldsymbol{\sigma} + \overline{\mathbf{C}}\mathbf{v_c} + \overline{\mathbf{G}} + \mathbf{\Phi}\tilde{\chi} \tag{19}$$

where, $\boldsymbol{\chi}$ and $\hat{\boldsymbol{\chi}}$ are the real and estimated parameters of the mobile manipulator, respectively, whereas $\tilde{\boldsymbol{\chi}} = \hat{\boldsymbol{\chi}} - \boldsymbol{\chi}$ is the vector of parameter errors.

In order to obtain the closed-loop equation for the inverse dynamics with uncertain model (2) is equated to (19),

$$\begin{aligned} &\overline{\mathbf{M}}\dot{\mathbf{v}} + \overline{\mathbf{C}}\mathbf{v} + \overline{\mathbf{G}} = \overline{\mathbf{M}}\sigma + \overline{\mathbf{C}}\mathbf{v_c} + \overline{\mathbf{G}} + \mathbf{\Phi}\tilde{\boldsymbol{\chi}} \\ &\overline{\mathbf{M}}(\boldsymbol{\sigma} - \dot{\mathbf{v}}) = -\overline{\mathbf{C}}\tilde{\mathbf{v}} - \mathbf{\Phi}\tilde{\boldsymbol{\chi}} \end{aligned} \tag{20}$$

and next, (17) is introduced in (20)

$$\dot{\tilde{\mathbf{v}}} = -\overline{\mathbf{M}}^{-1}\mathbf{\Phi}\tilde{\boldsymbol{\chi}} - \overline{\mathbf{M}}^{-1}\overline{\mathbf{C}}\tilde{\mathbf{v}} - \mathbf{L}_\mathbf{v} \tanh(\mathbf{L}_\mathbf{v}^{-1}\mathbf{K}_\mathbf{v}\tilde{\mathbf{v}}) \tag{21}$$

It is now introduced the following Lyapunov candidate function

$$V(\tilde{\mathbf{v}}, \tilde{\boldsymbol{\chi}}) = \frac{1}{2}\tilde{\mathbf{v}}^\mathbf{T}\mathbf{H}\overline{\mathbf{M}}\tilde{\mathbf{v}} + \frac{1}{2}\tilde{\boldsymbol{\chi}}^\mathbf{T}\gamma\tilde{\boldsymbol{\chi}} \tag{22}$$

where $\boldsymbol{\gamma} \in \Re^{lxl}$ is a positive definite diagonal matrix and $\mathbf{H}\overline{\mathbf{M}}$ is a symmetric and positive definite matrix. The time derivative of the Lyapunov candidate function is,

$$\begin{aligned} \dot{V}(\tilde{\mathbf{v}}, \tilde{\boldsymbol{\chi}}) = &-\tilde{\mathbf{v}}^\mathbf{T}\mathbf{H}\overline{\mathbf{M}}\mathbf{L}_\mathbf{v} \tanh\left(\mathbf{L}_\mathbf{v}^{-1}\mathbf{K}_\mathbf{v}\tilde{\mathbf{v}}\right) - \tilde{\mathbf{v}}^\mathbf{T}\mathbf{H}\overline{\mathbf{C}}\tilde{\mathbf{v}} - \tilde{\mathbf{v}}^\mathbf{T}\mathbf{H}\mathbf{\Phi}\tilde{\boldsymbol{\chi}} + \tilde{\boldsymbol{\chi}}^\mathbf{T}\gamma\dot{\tilde{\boldsymbol{\chi}}} \\ &+ \frac{1}{2}\tilde{\mathbf{v}}^\mathbf{T}\mathbf{H}\dot{\overline{\mathbf{M}}}\tilde{\mathbf{v}} \end{aligned}$$

Now, recalling that $\overline{\mathbf{M}}(\mathbf{q}) = \mathbf{H}^{-1}(\mathbf{M} + \mathbf{D})$ and $\overline{\mathbf{C}}(\mathbf{q}, \mathbf{v}) = \mathbf{H}^{-1}(\mathbf{C} + \mathbf{P})$,

$$\begin{aligned} \dot{V}(\tilde{\mathbf{v}}, \tilde{\boldsymbol{\chi}}) = &-\tilde{\mathbf{v}}^\mathbf{T}\mathbf{H}\overline{\mathbf{M}}\mathbf{L}_\mathbf{v} \tanh\left(\mathbf{L}_\mathbf{v}^{-1}\mathbf{K}_\mathbf{v}\tilde{\mathbf{v}}\right) - \tilde{\mathbf{v}}^\mathbf{T}(\mathbf{C} + \mathbf{P})\tilde{\mathbf{v}} - \tilde{\mathbf{v}}^\mathbf{T}\mathbf{H}\mathbf{\Phi}\tilde{\boldsymbol{\chi}} + \tilde{\boldsymbol{\chi}}^\mathbf{T}\gamma\dot{\tilde{\boldsymbol{\chi}}} \\ &+ \frac{1}{2}\tilde{\mathbf{v}}^\mathbf{T}\dot{\mathbf{M}}\tilde{\mathbf{v}} \end{aligned}$$

Due to the well known skew-symmetric property of $(\dot{\mathbf{M}} - 2\mathbf{C}), \dot{V}(\tilde{\mathbf{v}}, \tilde{\boldsymbol{\chi}})$ reduces to,

$$\begin{aligned} \dot{V}(\tilde{\mathbf{v}}, \tilde{\boldsymbol{\chi}}) = &-\tilde{\mathbf{v}}^\mathbf{T}\mathbf{H}\overline{\mathbf{M}}\mathbf{L}_\mathbf{v} \tanh\left(\mathbf{L}_\mathbf{v}^{-1}\mathbf{K}_\mathbf{v}\tilde{\mathbf{v}}\right) - \tilde{\mathbf{v}}^\mathbf{T}\mathbf{P}\tilde{\mathbf{v}} - \tilde{\mathbf{v}}^\mathbf{T}\mathbf{H}\mathbf{\Phi}\tilde{\boldsymbol{\chi}} \\ &+ \tilde{\boldsymbol{\chi}}^\mathbf{T}\gamma\dot{\tilde{\boldsymbol{\chi}}} \end{aligned} \tag{23}$$

The proposed parameter-updating law for the adaptive dynamic compensation controller is based on a leakage term, or σ-modification [21–23]. By including such term, the obtained robust updating law is

$$\dot{\tilde{\boldsymbol{\chi}}} = \gamma^{-1}\mathbf{\Phi}^\mathbf{T}\mathbf{H}\tilde{\mathbf{v}} - \gamma^{-1}\mathbf{\Gamma}\tilde{\boldsymbol{\chi}} \tag{24}$$

where $\mathbf{\Gamma} \in \Re^{lxl}$ is a diagonal positive gain matrix. Notice that (24) can be rewritten as

$$\dot{\tilde{\boldsymbol{\chi}}} = \gamma^{-1}\mathbf{\Phi}^\mathbf{T}\mathbf{H}\tilde{\mathbf{v}} - \gamma^{-1}\mathbf{\Gamma}\tilde{\boldsymbol{\chi}} - \gamma^{-1}\mathbf{\Gamma}\boldsymbol{\chi} \tag{25}$$

Let us now consider that the dynamic parameters can vary, *i.e.*, $\boldsymbol{\chi} = \boldsymbol{\chi}(t)$ and $\dot{\tilde{\boldsymbol{\chi}}} = \dot{\hat{\boldsymbol{\chi}}} - \dot{\boldsymbol{\chi}}$. Substituting (25) in (23),

$$\dot{V}(\tilde{\mathbf{v}}, \tilde{\boldsymbol{\chi}}) = -\tilde{\mathbf{v}}^\mathbf{T}\mathbf{H}\overline{\mathbf{M}}\mathbf{L}_\mathbf{v} \tanh\left(\mathbf{L}_\mathbf{v}^{-1}\mathbf{K}_\mathbf{v}\tilde{\mathbf{v}}\right) - \tilde{\mathbf{v}}^\mathbf{T}\mathbf{P}\tilde{\mathbf{v}} - \tilde{\boldsymbol{\chi}}^\mathbf{T}\mathbf{\Gamma}\tilde{\boldsymbol{\chi}} - \tilde{\boldsymbol{\chi}}^\mathbf{T}\mathbf{\Gamma}\boldsymbol{\chi} - \tilde{\boldsymbol{\chi}}^\mathbf{T}\gamma\dot{\boldsymbol{\chi}} \tag{26}$$

Considering small values of $\tilde{\mathbf{v}}$, then $\mathbf{L}_\mathbf{v} \tanh\left(\mathbf{L}_\mathbf{v}^{-1}\mathbf{K}_\mathbf{v}\tilde{\mathbf{v}}\right) \approx \mathbf{K}_\mathbf{v}\tilde{\mathbf{v}}$. The following constants are defined: $\upsilon_\Gamma = k_{\max}(\mathbf{\Gamma})$, $\upsilon_\gamma = k_{\max}(\gamma)$, $\mu_\Gamma = \chi(\mathbf{\Gamma}), \mu_{\overline{M}K_vP} = \chi(\mathbf{H}\overline{\mathbf{M}}\mathbf{K}_\mathbf{v}) + \chi(\mathbf{P})$, where $\chi(\mathbf{Z}) = \sqrt{\lambda_{min}(\mathbf{Z}^\mathbf{T}\mathbf{Z})}$ is

Fig. 5. Experimental framework for a dynamic visual feedback system for mobile manipulator.

the minimun singular value to $\mathbf{Z}$, $k_{max}(\mathbf{Z}) = \sqrt{\lambda_{max}(\mathbf{Z}^{\mathbf{T}}\mathbf{Z})}$ denotes the maximum singular value of $\mathbf{Z}$, and $\lambda_{\min}(.)$ and $\lambda_{\max}(.)$ represent the smallest and the biggest eigenvalues of a matrix, respectively. Then, $\dot{V}$ can be rewritten as,

$$\dot{V}(\tilde{\mathbf{v}},\tilde{\boldsymbol{\chi}}) = -\mu_{\overline{M}K_vP}\|\tilde{\mathbf{v}}\|^2 - \mu_\Gamma\|\tilde{\boldsymbol{\chi}}\|^2 + \upsilon_\Gamma\|\tilde{\boldsymbol{\chi}}\|\|\boldsymbol{\chi}\| + \upsilon_\gamma\|\tilde{\boldsymbol{\chi}}\|\|\dot{\boldsymbol{\chi}}\| \tag{27}$$

Considering $\zeta \in \Re^+$ is a difference square

$$\left(\frac{1}{\zeta}\|\tilde{\boldsymbol{\chi}}\| - \zeta\|\boldsymbol{\chi}\|\right)^2 = \frac{1}{\zeta^2}\|\tilde{\boldsymbol{\chi}}\|^2 - 2\|\tilde{\boldsymbol{\chi}}\|\|\boldsymbol{\chi}\| + \zeta^2\|\boldsymbol{\chi}\|^2$$

can be written as

$$\|\tilde{\boldsymbol{\chi}}\|\|\boldsymbol{\chi}\| \leqslant \frac{1}{2\zeta^2}\|\tilde{\boldsymbol{\chi}}\|^2 + \frac{\zeta^2}{2}\|\boldsymbol{\chi}\|^2 \tag{28}$$

By applying a similar reasoning with $\eta \in \Re^+$, it can be obtained

$$\|\tilde{\boldsymbol{\chi}}\|\|\dot{\boldsymbol{\chi}}\| \leqslant \frac{1}{2\eta^2}\|\tilde{\boldsymbol{\chi}}\|^2 + \frac{\eta^2}{2}\|\dot{\boldsymbol{\chi}}\|^2 \tag{29}$$

Substituting (29) and (28) in (27)

$$\dot{V}(\tilde{\mathbf{v}},\tilde{\boldsymbol{\chi}}) \leqslant -\mu_{\overline{M}K_vP}\|\tilde{\mathbf{v}}\|^2 - \mu_\Gamma\|\tilde{\boldsymbol{\chi}}\|^2 + \upsilon_\Gamma\left(\frac{1}{2\zeta^2}\|\tilde{\boldsymbol{\chi}}\|^2 + \frac{\zeta^2}{2}\|\boldsymbol{\chi}\|^2\right) + \upsilon_\gamma\left(\frac{1}{2\eta^2}\|\tilde{\boldsymbol{\chi}}\|^2 + \frac{\eta^2}{2}\|\dot{\boldsymbol{\chi}}\|^2\right) \tag{30}$$

Eq. (30) can be written in compact form as

$$\dot{V}(\tilde{\mathbf{v}},\tilde{\boldsymbol{\chi}}) \leqslant -\alpha_1\|\tilde{\mathbf{v}}\|^2 - \alpha_2\|\tilde{\boldsymbol{\chi}}\|^2 + \rho \tag{31}$$

where, $\alpha_1 = \mu_{\overline{M}K_vP} > 0, \alpha_2 = \mu_\Gamma - \frac{\mu_\Gamma}{2\zeta^2} - \frac{\mu_\gamma}{2\eta^2} > 0$ and $\rho = \upsilon_\Gamma\frac{\zeta^2}{2}\|\boldsymbol{\chi}\|^2 + \upsilon_\gamma\frac{\eta^2}{2}\|\dot{\boldsymbol{\chi}}\|^2$, with ζ and η conveniently selected. Now, from the Lyapunov candidate function $V(\tilde{\mathbf{v}},\tilde{\boldsymbol{\chi}}) = \frac{1}{2}\tilde{\mathbf{v}}^{\mathbf{T}}\mathbf{H}\overline{\mathbf{M}}\tilde{\mathbf{v}} + \frac{1}{2}\tilde{\boldsymbol{\chi}}^{\mathbf{T}}\boldsymbol{\gamma}\tilde{\boldsymbol{\chi}}$ it can be stated that

$$V \leqslant \beta_1\|\tilde{\mathbf{v}}\|^2 + \beta_2\|\tilde{\boldsymbol{\chi}}\|^2 \tag{32}$$

where $\beta_1 = \frac{1}{2}\vartheta_{\overline{M}}$, $\beta_2 = \frac{1}{2}\vartheta_\gamma$, $\vartheta_{\overline{M}} = k_{max}(\mathbf{H}\overline{\mathbf{M}})$, $\vartheta_\gamma = k_{max}(\boldsymbol{\gamma})$. Then,

$$\dot{V} \leqslant -\Lambda V + \rho \tag{33}$$

with $\Lambda = \left\{\frac{\alpha_1}{\beta_1}, \frac{\alpha_2}{\beta_2}\right\}$. Since ρ is bounded, (33) implies that $\tilde{\mathbf{v}}(t)$ and $\tilde{\boldsymbol{\chi}}(t)$ are finally bounded. Therefore, the σ modification term makes the adaptation law more robust at the expense of increasing the error bound. As ρ is a function of the minimum singular value of the gain matrix $\boldsymbol{\Gamma}$ of the σ modification term, and its values are arbitrary, then the error bound can be made small. In the limit, if $\boldsymbol{\Gamma} \to \mathbf{0}$, then $\tilde{\mathbf{v}}(t) \to \mathbf{0}$ as $t \to \infty$, as previously shown.

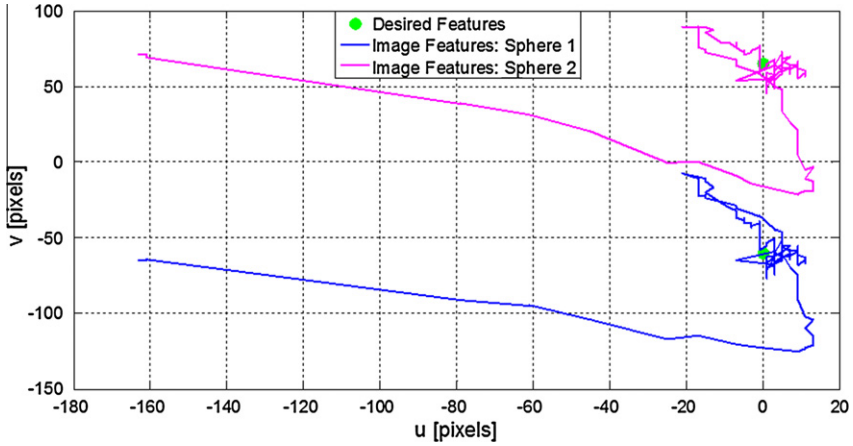

Fig. 6. Image features trajectories.

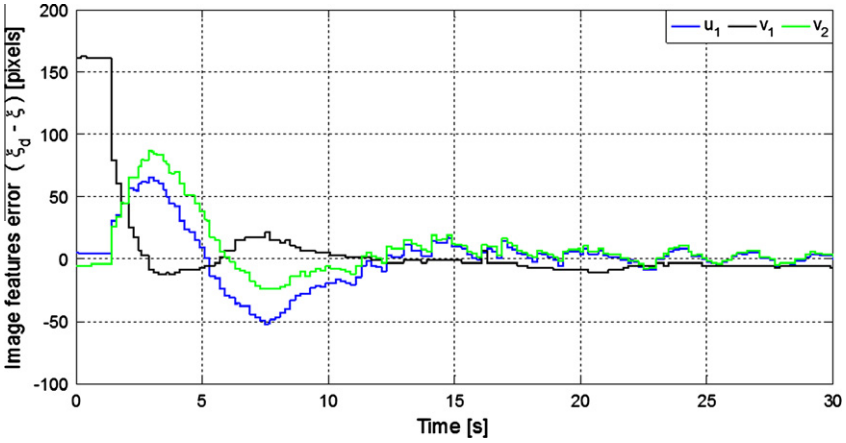

Fig. 7. Time evolution C.

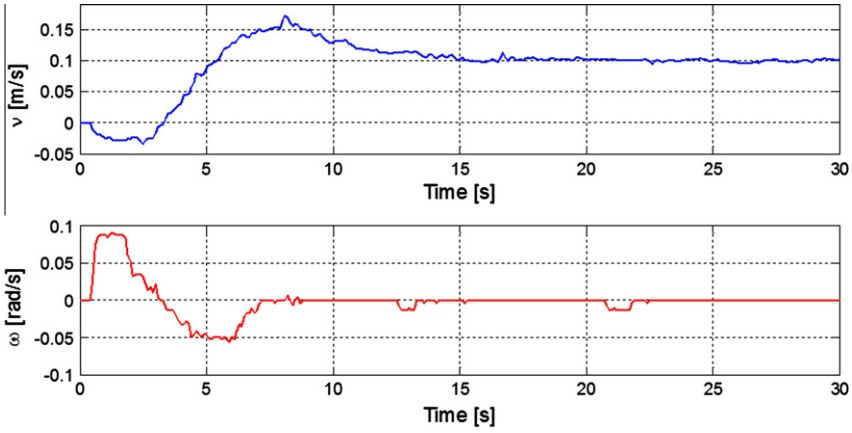

Fig. 8. Velocity commands to the mobile platform.

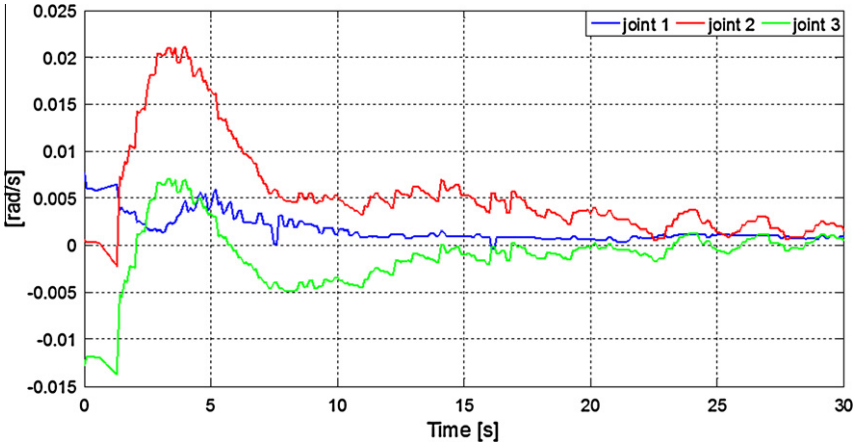

Fig. 9. Joint velocity commands to the robotic arm.

Remark 1. Note that the updating law (24) needs the **H** matrix. This matrix includes parameters of the actuators, which can be easily known and remain constant. Therefore, this is not a relevant constraint within the adaptive control design.

4. Stability and robustness analysis

The proposed controller presented above considers that the velocity of the object to be followed ${}^{w}\dot{\mathbf{p}}$ is exactly known. Nevertheless, this is not always possible in a real context. In practice, this velocity will be estimated by using the visual position sensing of the object, for instance by an $\alpha - \beta$ filter [24]. This motivates to study the image feature error $\tilde{\xi}$ behaviour by considering the estimated velocity errors of the object to be followed and also relaxing the assumption of perfect velocity tracking.

It is defined the estimation velocity errors of the object into the image plane as,

$$\boldsymbol{\varepsilon} = \mathbf{J}_{\mathbf{o}}({}^{w}\hat{\dot{\mathbf{p}}} - {}^{w}\dot{\mathbf{p}})$$

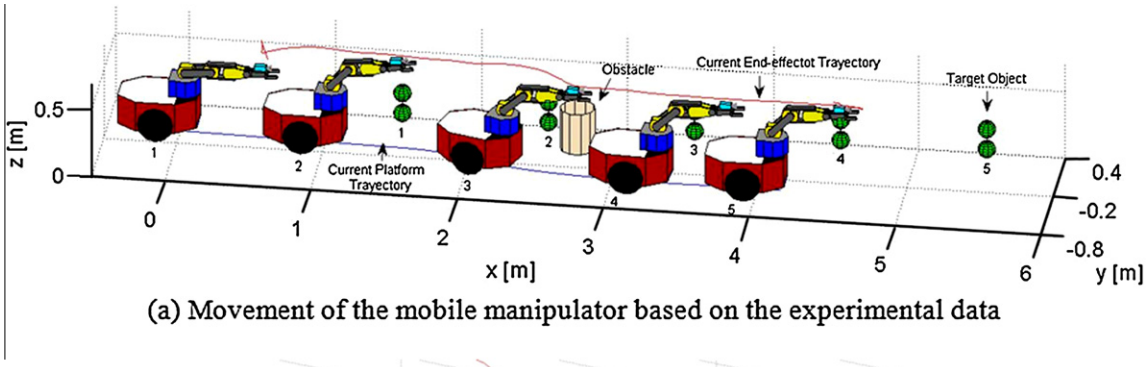

(a) Movement of the mobile manipulator based on the experimental data

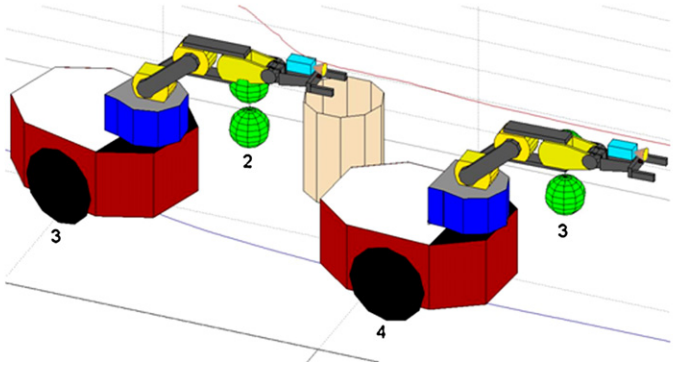

Fig. 10. Movement of the mobile manipulator based on the experimental data The position of the mobile manipulator and the position of the target at the same instant are shown. Five different time instants are depicted.

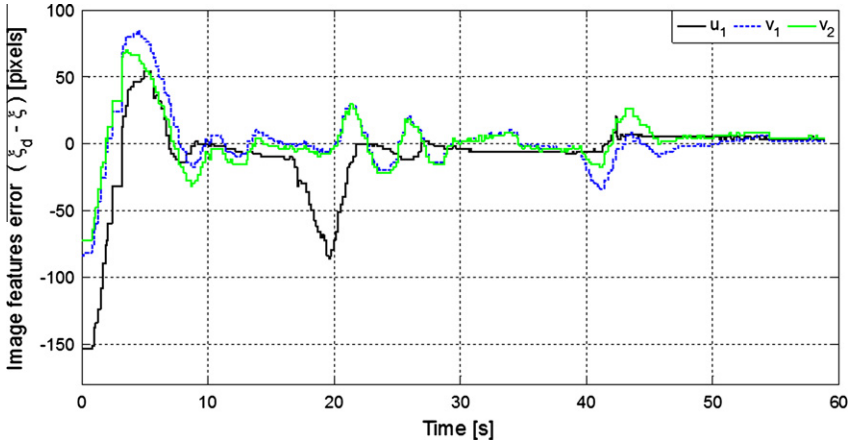

Fig. 11. Time evolution £.

where ${}^{w}\dot{\mathbf{p}}$ and $\hat{\dot{\mathbf{p}}}$ are the real and estimated velocities of the object, respectively. Hence (13) can now be written as

$$\dot{\tilde{\xi}} + \mathbf{L}_{\mathbf{K}} \tanh\left(\mathbf{L}_{\mathbf{K}}^{-1}\mathbf{K}\,\tilde{\xi}\right) = \mathbf{J}\tilde{\mathbf{v}} + \boldsymbol{\varepsilon} \tag{34}$$

Lyapunov candidate function (14) is considered again, which time derivative along the trajectories of the system (34) is

$$\dot{V}(\tilde{\xi}) = \tilde{\xi}^{\mathbf{T}}(\mathbf{J}\tilde{\mathbf{v}} + \boldsymbol{\varepsilon}) - \tilde{\xi}^{\mathbf{T}}\mathbf{L}_{\mathbf{K}} \tanh\left(\mathbf{L}_{\mathbf{K}}^{-1}\mathbf{K}\,\tilde{\xi}\right) \tag{35}$$

A sufficient condition for $\dot{V}(\tilde{\xi})$ to be negative definite is

$$\left|\tilde{\xi}^{\mathbf{T}}\mathbf{L}_{\mathbf{K}} \tanh\left(\mathbf{L}_{\mathbf{K}}^{-1}\mathbf{K}\,\tilde{\xi}\right)\right| > |\tilde{\xi}^{\mathbf{T}}(\mathbf{J}\tilde{\mathbf{v}} + \boldsymbol{\varepsilon})| \tag{36}$$

For large values of $\tilde{\xi}$, it can be considered that $\mathbf{L}_{\mathbf{K}} \tanh(\mathbf{L}_{\mathbf{K}}^{-1}\mathbf{K}\,\tilde{\xi}) \approx \mathbf{L}_{\mathbf{K}}$. Then, (36) can be expressed as

$$\|\mathbf{L}_{\mathbf{K}}\| > \|\mathbf{J}\tilde{\mathbf{v}} + \boldsymbol{\varepsilon}\| \tag{37}$$

thus making the errors $\tilde{\xi}$ decrease.

Now, for small values of $\tilde{\xi}$, $\mathbf{L}_{\mathbf{K}} \tanh\left(\mathbf{L}_{\mathbf{K}}^{-1}\mathbf{K}\,\tilde{\xi}\right) \approx \mathbf{K}\tilde{\xi}$, thus (36) can be written as,

$$\|\tilde{\xi}\| > \frac{\|\mathbf{J}\tilde{v} + \boldsymbol{\varepsilon}\|}{\lambda_{\min}(\mathbf{K})}$$

thus implying that the error $\tilde{\xi}$ is bounded by,

$$\|\tilde{\xi}\| \leqslant \frac{\|\mathbf{J}\tilde{\mathbf{v}} + \boldsymbol{\varepsilon}\|}{\lambda_{\min}(\mathbf{K})} \tag{38}$$

Hence, it is concluded that the image feature error is ultimately bounded by the bound $\|\mathbf{J}\tilde{\mathbf{v}} + \boldsymbol{\varepsilon}\|/\lambda_{min}(\mathbf{K})$ on a norm of the control error and the estimated velocity error of the object to be followed.

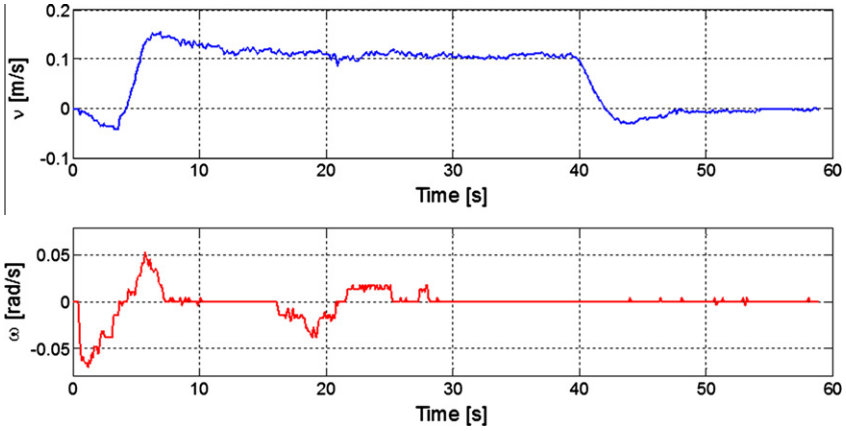

Fig. 12. Velocity commands to the mobile platform.

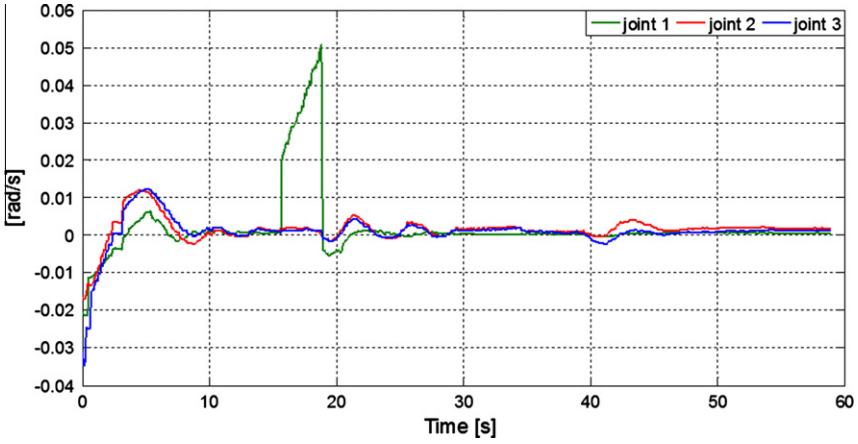

Fig. 13. Joint velocity commands to the robotic arm.

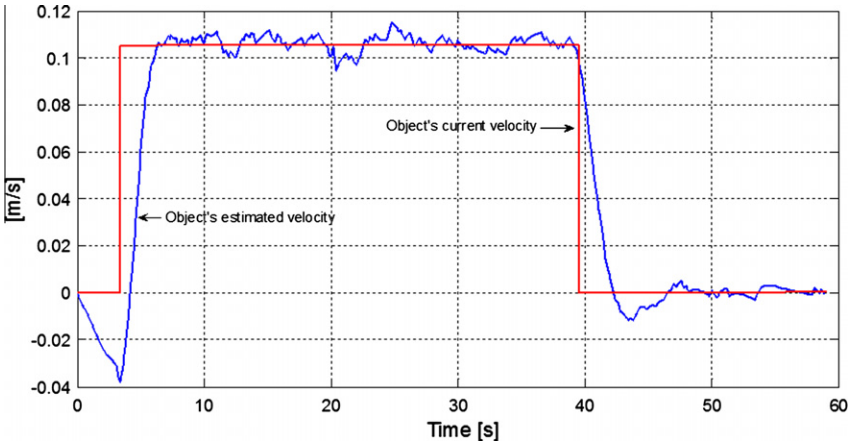

Fig. 14. Estimation of the object's velocity.

5. Experimental results

In order to evaluate the performance of the proposed controller, several experiments were carried out for visual control for 3D target tracking of a mobile manipulator. The target to be tracked is mounted on another mobile platform PIONEER 3DX as Fig. 5b shows. Most representative results are presented in this section. The 6 DOF experimental system used in the experiments is shown in Fig. 5a, which is composed of a nonholonomic mobile platform PIONEER 3AT, a laser rangefinder mounted on it, a robotic arm CYTON Alpha 7 DOFs (only 3 DOF of the 7 available DOFs are used in the experiments), and a Mini CMOS Camera JK-805 with 1/3" Video Sensor.

Dynamic adaptive compensation is performed for the mobile platform alone, because it presents the most significant dynamics of the whole mobile manipulator system.

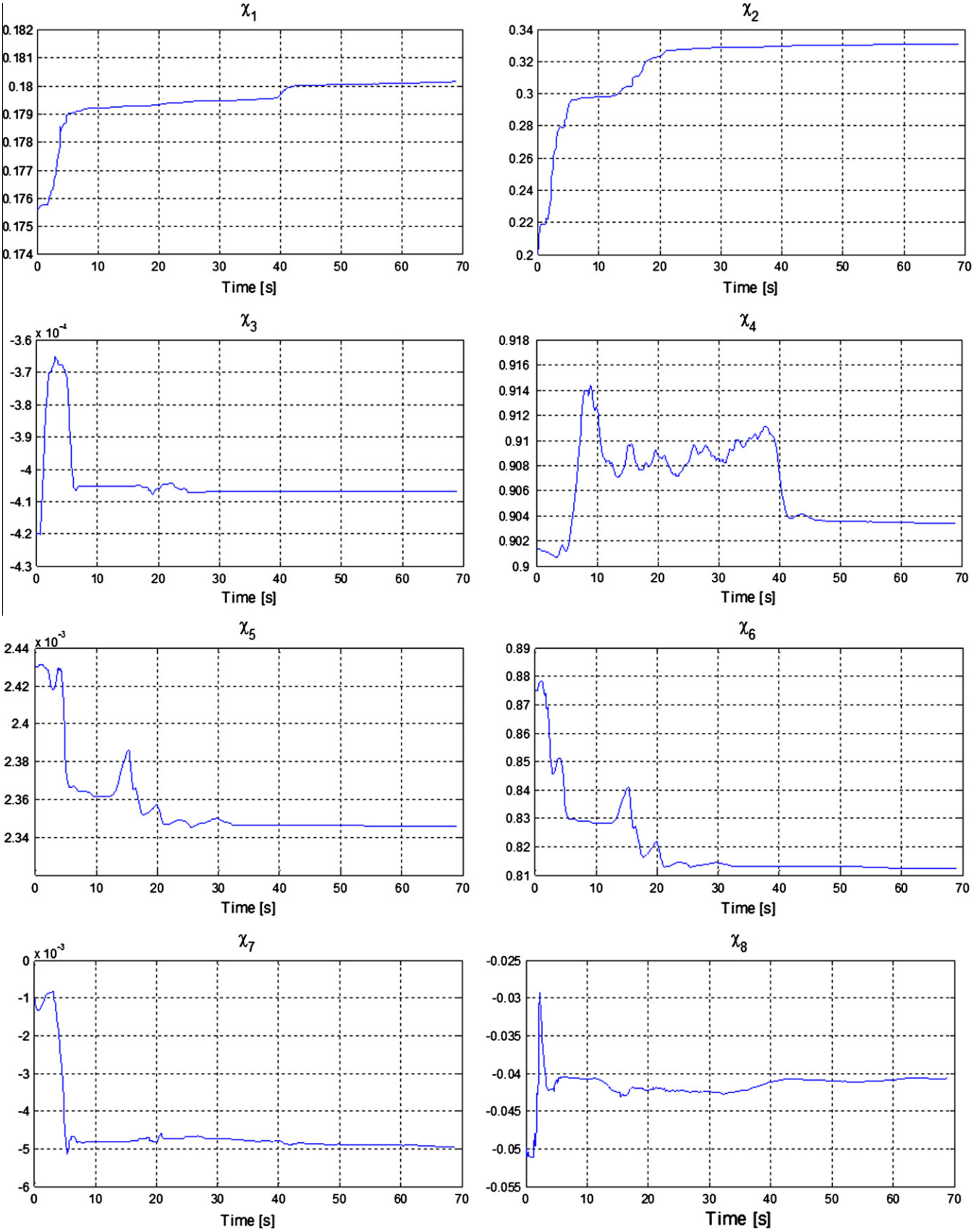

Fig. 15. Evolution of the adaptive parameter *.

For all experiments in this section it was considered an error of 25% in model parameters. Also, the positions of the arm joints that maximize the arm's manipulability are obtained through numeric simulation. This way, the desired joint angles are: $\theta_{1d} = 0$[rad],

$\theta_{2d} = 0.6065$[rad], and $\theta_{3d} = -1.2346$[rad]. Matrix H used in the updating law is $\mathbf{H} = diag\,(33.4, 16.7)$. Also, controller's gain matrices are set to: $\mathbf{K} = diag(0.12, 0.12, 0.12)$; $\mathbf{L_K} = diag(0.15, 0.15, 0.15)$; $\mathbf{D} = diag(0.14, 0.2, 0.02, 0.02, 0.02)$; $\mathbf{L_D} = diag(0.7, 1, 0.1, 0.1, 0.1)$.

Experiment I: In this experiment, the mobile platform location is $\mathbf{q}_p = [0\text{ m }\ 0\text{ m }\ 0\text{ rad}]^T$ and the robotic arm configuration is $\mathbf{q}_a = [-0.18\ 0\ 0]^T$ [rad]; thus, considering that the origin of the image coordinates is located at the centre of the image, the initial values of image features initial are $\xi(0) = [u_1\ v_1\ v_2]^T = [-162\ -70\ 68]^T$ [pixels]. The desired image features vector was defined as $\xi_d = [u_1\ v_1\ v_2]^T = [0\ -60\ 65]^T$ [pixels]. Figs. 6–9 show the results of the first experiment. Fig. 6 shows the evolution of the image features on the image plane. Fig. 7 shows that the control errors $\tilde{\xi}(t)$ are ultimately bounded with final values close to zero, i.e. achieving final feature errors max $(|\xi_i|) < 5$ pixels; while Figs. 8 and 9 show the control actions of the mobile manipulator.

Experiment II: Obstacle avoidance and maximum manipulability control are considered in this experiment. It is considered that the obstacle is placed up to a maximum height that does not interfere with the vision camera, so that the end-effector can follow the target object even when the platform is avoiding the obstacle. Hence, the task is divided into two different control objectives, i.e., a principal objective: *moving target object tracking*; and a secondary objective, achieved by taking advantage of the redundancy of the mobile manipulator as explained in Section 3: *obstacle avoidance and maximum manipulability control.* The image features initial vector is $\xi(0) = [u_1\ v_1\ v_2]^T = [156\ 22\ 134]^T$[pixels]. The desired image features vector is defined as $\xi_d = [u_1\ v_1\ v_2]^T = [0\ -50\ 50]^T$ [pixels]. It is important to remark that, similar to previous experiment, the origin of the image coordinates is located at the centre of the image. Figs. 10–15 show the results of the second experiment. From the Fig. 13 and 14 ($15 < t < 25$[s] approximately) it becomes apparent that the end-effector tracks the moving target object while avoiding the obstacle. Fig. 10 shows the stroboscopic movement on the X–Y–Z space. It can be seen the good performance of the proposed control system. Fig. 11 shows that the control errors $\tilde{\xi}(t)$ are ultimately bounded with final values close to zero, i.e. achieving final feature errors max $(|\xi_i|) < 4$ pixels; Figs. 12 and 13 show the control actions of the robot, while Fig. 14 represents the estimation of the object's velocity. Notice that even with large velocity estimation errors, like the errors which appear at the beginning of the experiment, the control errors remain bounded. Finally Fig. 15 shows the evolution of the adaptive parameters, where it can be seen that all the parameters converge to fixed values.

6. Conclusions

In this paper an adaptive dynamic visual feedback control for mobile manipulators for 3D target tracking has been developed. It was considered the redundancy of the mobile manipulator system to control the manipulability and for obstacle avoidance. It has been also proposed an adaptive controller which updates the mobile manipulator dynamics on-line. The design of the whole controller was based on two cascaded subsystems: a minimum norm visual servo kinematic controller which complies with the 3D target tracking objective, and an adaptive dynamic compensation controller that compensates the dynamics of the mobile manipulator. Both the kinematic controller and the adaptive dynamic controller have been designed to prevent from command saturation. Robot commands were defined in terms of reference velocities. Stability and robustness are proved by considering the Lyapunov's method. The performance of the proposed controller is shown through real experiments.

References

[1] Siegwart R, Nourbakhsh I. Introduction to autonomous mobile robots. The MIT Press; 2004.
[2] Khatib O. Mobile manipulation: the ronotic assistant. Robots Auton Syst 1999;26(2/3):175–83.
[3] Das Y, Russell R, Kircanski N, Goldenberg A. An articulated robotic scanner for mine detection – a novel approach to vehicle mounted systems. In: Proceedings of the SPIE conference, Orlando, Florida; 1999. p. 5–9
[4] Hutchinson S, Hager GD, Corke PI. A tutorial on visual servo control. IEEE Trans Robot Automat 1996;12(5):651–70.
[5] Luca AD, Oriolo G, Giordano PR. Image-based visual servoing schemes for nonholonomic mobile manipulators. Robotica 2007;25(2):131–45.
[6] Muis A, Ohnishi A. Eye-to-hand approach on eye-in-hand configuration within real-time visual servoing. IEEE/ASME Trans Mechatron 2005;10. 404-4010.
[7] Wang Ying, Lang Haoxiang, de Silva Clarence W. A hybrid visual servo controller for robust grasping by wheeled mobile robots. IEEE/ASME Trans Mechatron 2009.
[8] Mansard N, Stasse O, Chaumette F, Yokoi K. Visually-guided grasping while walking on a humanoid robot. In: Proc. IEEE int. conf. robot. autom., Rome, Italy; April 2007. p. 3041–7.
[9] Yoo WS, Kim J-D, Na SJ. A study on a mobile platform-manipulator welding system for horizontal fillet joints. Mechatronics 2001;11(7):853–68.
[10] Cetin Levent, Uyar Erol. Design and control of a mobile manipulator with stereo vision guidance. Int J Mechatron Manuf Syst 2009;2(3):369–82.
[11] Xu De, Tan Min, Shen Yang. A new simple visual control method based on cross ratio invariance. In: International conference on mechatronics & automation; July 2005. p. 370–5.
[12] Andaluz Víctor, Roberti Flavio. Robust control with redundancy resolution and dynamic compensation for mobile manipulators. In: IEEE-ICIT international conference on industrial technology; 2010. p. 1449–54.
[13] Slotine J-JE, Li Weiping. Applied nonlinear control. Englewood Cliffs, New Jersey: hentice-Hall; 1991.
[14] Sciavicco L, Siciliano B. Modelling and control of robot manipulators. Springer; 2000. p. 84–106.
[15] Hu YM, Guo BH. Modeling and motion planning of a three-link wheeled mobile manipulator. In: International conference on control, automation and vision; 2004. p. 993–8.
[16] Chaumette F, Rives P, Espiau B. Classification and realization of the different vision-based tasks. In: Hashimoto K, editor. Visual servoing. Singapore: World Scientific; 1993. p. 199–228.
[17] Hashimoto K, Aoki A, Noritsugu T. Visual servoing with redundant features. In: Proc. 35th conf. decision and control, Kobe, Japan; December 1996. p. 2482–3.
[18] Weiss LE, Sanderson AC, Neuman CP. Dynamic sensor-based control of robots with visual feedback. IEEE J Robot Automat 1987;3:404–17.
[19] Yoshikawa T. Manipulability of robotic mechanisms. Int J Robot Res 1985;4(2):3–9.
[20] Bayle B, Fourquet J-Y. Manipulability analysis for mobile manipulators. In: IEEE international conference on robots & automation; 2001. p. 1251–6.
[21] Kaufman H, Barkana I, Sobel K. Direct adaptive control algorithms, theory and applications. 2nd ed. New York, USA: Ed: Springer; 1998.
[22] Sastry S, Bodson M. Adaptive control-stability, convergence and robustness. Englewood Cliffs, NJ: Prentice-Hall; 1989.
[23] Nasisi O, Carelli R. Adaptive servo visual robot control. Robot Auton Syst 2003;43:51–78.
[24] Kalata P. The tracking index: a generalized parameter for $\alpha - \beta$ and $\alpha - \beta - \gamma$ target trackers. IEEE Trans Aero Electron Syst 1994;20(2):174–82.
[25] Bayle B, Fourquet J-Y, Renaud M. Manipulability of wheeled mobile manipulators: application to motion generation. Int J Robot Res 2003;22(7):8565–81.